Journal of Power Sources 261 (2014) 188–197

Contents lists available at ScienceDirect

Journal of Power Sources

journal homepage: www.elsevier.com/locate/jpowsour

Preparation and electrochemical properties of $Li_3V_{1.8}Mn_{0.2}(PO_4)_3$ doped via different Mn sources

Lin Chen [a,b], Bo Yan [a], Yafeng Xie [b], Shaoming Wang [a], Xuefan Jiang [b], Gang Yang [a,b,*]

[a] School of Material Science and Engineering, Jiangsu University of Science and Technology, Zhenjiang 212003, China
[b] Jiangsu Laboratory of Advanced Functional Material, Changshu Institute of Technology, Changshu 215500, China

HIGHLIGHTS

- Mn-doped LVP composites (LVMP) synthesized using various manganese sources.
- Manganese with valences +3 and +4 successfully inserted $Li_3V_2(PO_4)_3$ without impurity.
- LVMP doped by MnOOH delivers 137 mAh g^{-1} near theoretical capacity and remains 98% after 50 cycles.
- MnOOH is a prefer dopant to improve the electrochemical properties of LVP.

ARTICLE INFO

Article history:
Received 31 December 2013
Received in revised form
21 February 2014
Accepted 17 March 2014
Available online 26 March 2014

Keywords:
Lithium batteries
Cathode materials
Substitution
Lithium vanadium phosphate

ABSTRACT

This work attempts to substitute V of $Li_3V_2(PO_4)_3$ (LVP) by the doped ion of manganese with the valence of +2, +3 and +4 and various ionic radiuses. A series of Mn-doped LVP composites (LVMP) by different manganese sources are synthesized by sol–gel and heat-treatment. Manganese ion with the valences of +3 and +4 have been successfully inserted into the lattice of $Li_3V_2(PO_4)_3$ to form a stable solid-solution even the substitution mole ratio reaches to 0.2, except the impurity phase of $LiMnPO_4$ in LVMP when manganese ions with the valence of +2 involve in the substitution. Mn^{2+} exists in all three samples as expected, but the main valence state of Mn ions in LVMP-A, LVMP-B and LVMP-C are Mn^{4+}, Mn^{3+} and Mn^{2+}, respectively. LVMP-B (MnOOH as dopant) delivers the highest capacity of 137 mAh g^{-1}, than LVMP-A (MnO_2 as dopant) 125 mAh g^{-1} and LVMP-C (Mn_3O_4 as dopant) 123 mAh g^{-1}. LVMP-B shows the best cycle performance, remaining 98% of the initial capacity after 50 cycles in range 3.0–4.3 V. Mn source of MnOOH properly substituted the structure of LVP enhances the lithium diffusion ability and stability of LVP during charge/discharge.

1. Introduction

Numerous efforts have been made on the development of framework materials based on the phosphate polyanion. Monoclinic $Li_3V_2(PO_4)_3$ (LVP) with both mobile Li^+ cations and redox-active metal sites located within a rigid phosphate framework, become attractive candidates owning to its high theoretical discharge capacity of 197 mAh g^{-1} (3.0–4.8 V) and characteristics three-dimensional pathways for Li^+ extraction and re-insertion [1,2]. The strong P–O bonds and three-dimensional (3D) solid framework in $(PO_4)^{3-}$ anions can guarantee both the dynamic and thermal stability required to fulfill the safety features in high power applications, such as electric vehicles (EVs) and hybrid electric vehicles (HEVs) [3].

However, the critical disadvantage of poor electronic and ionic conductivities limit the application fields of $Li_3V_2(PO_4)_3$ [4–6]. Improvements of poor conductivity have been achieved, such as synthesizing nanoparticles, forming electrically conductive coating on materials, and doping cations in the Li or V site to improve electrochemical properties. Metal ion doping is a convenient way to improve the electrochemical performance of $Li_3V_2(PO_4)_3$. A lot of cations have been employed to dope $Li_3V_2(PO_4)_3$, and some positive impacts are reported on its electrochemical performance. V^{3+} has been partially substituted with isovalent or aliovalent metal ions, such as Nb^{5+} [7], Ti^{4+} [8], Zr^{4+} [9], Fe^{3+} [10], Al^{3+} [11,12], Ce^{3+} [13], Cr^{3+} [14], Sc^{3+} [15], Y^{3+} [16], Mg^{2+} [17,18], Mn^{2+} [19,20], Co^{2+} [21]

* Corresponding author. Jiangsu Laboratory of Advanced Functional Material, Changshu Institute of Technology, Changshu 215500, China.
Tel.: +86 512 52251895; fax: +86 512 52251842.
E-mail addresses: gyang@cslg.edu.cn, gangyang@ua.pt (G. Yang).

http://dx.doi.org/10.1016/j.jpowsour.2014.03.061
0378-7753/

and Na^+ [3]. The modified NASICON structure and the electro chemical performance of LVP are quite dependent on the doping elemental structure besides doping content.

Manganese is an interesting substitute in NASICON structure of LVP, because Mn-based materials, such as $LiMnO_2$, Li_2MnO_3, $LiNi_{1/3}Co_{1/3}Mn_{1/3}O_2$, have been widely studied as cathode materials for lithium batteries [22–26]. M. Bini et al. [20] reported that a solubility limit ($x = 0.124$) was determined for Mn(II) doped LVP via sol–gel route, generating the smaller irreversible capacity for LVP. In the previous work, the ionic radius of various doping elements is an important factor to the crystal structure and electrochemical properties [15,27,28]. But the doping structure and electrochemical properties of LVP are unknown after the precursor of the doped ion manganese with valence of +2, +3, and +4, respectively.

In this work, we attempt to substitute V by the doped ion of manganese with the valence of +2, +3 and +4 and various ionic radiuses. $(CH_3COO)_2Mn\cdot 4H_2O$ and MnO_2 as +2 and +4 manganese sources are commercial, and MnOOH and Mn_3O_4 as +3 and +2/+3 manganese source are synthesized before as doping precursors. A series of Mn-doped $Li_3V_2(PO_4)_3$ composites by different manganese sources are synthesized and their electrochemical properties are discussed in detail.

2. Experiment

2.1. Synthesis of MnOOH nanorods

MnOOH was prepared via a facile hydrothermal treatment as the previous work. $KMnO_4$ was first fully dissolved in deionized water under room temperature, and then ethanol added. After vigorous stirring for 30 min, the suspension was transferred into Teflon-lined stainless steel autoclave. The sealed autoclave was heated in an oven at 140 °C for 24 h. The product was centrifuged, washed with deionized water and absolute alcohol. MnOOH was obtained after drying at 80 °C in vacuum.

2.2. Synthesis of Mn_3O_4 nanoparticles

6 mmol $MnCl_2\cdot 4H_2O$ (1.2 g) added into 60 mL ethanol amine (ETA), the mixture was operated in a 600 W ultrasonic reactor for 4 h [29]. Then 100 mL distilled water was added into the resulting colloid solution. After constantly stirred at room temperature for 5 h, the clear brown mixture turned to a dark brown suspension. The suspension was centrifuged at 8000 rpm for 5 min and washed repeatedly with H_2O to remove the residual ETA until the pH of the filtrate was neutral. The Mn_3O_4 nanoparticles were dried at 80 °C in vacuum, and collected as a dark brown powder.

2.3. Synthesis of $Li_3V_{1.8}Mn_{0.2}(PO_4)_3$

The $Li_3V_{1.8}Mn_{0.2}(PO_4)_3$ composites (LVMP) were prepared by a sol–gel method [1]. All chemicals used in this work were of analytical grade. V_2O_5, $NH_4H_2PO_4$, Li_2CO_3, MnO_2, $(CH_3COO)_2Mn\cdot 4H_2O$ and oxalic acid were used as raw materials. First, V_2O_5 and oxalic acid in a stoichiometric ratio of 1:3 were dissolved in deionized water under magnetic stirring at 80 °C until a clear blue solution was formed. Oxalic acid was used both as a chelating agent and reducing agent. Then a mixture of stoichiometric $NH_4H_2PO_4$, MnO_2 (or MnOOH, Mn_3O_4, $(CH_3COO)_2Mn\cdot 4H_2O$) and Li_2CO_3 was added to the solution, and this batch was vigorously stirred for 10 min at 80 °C. Citric acid was then added to the mixed solution. The mixture was stirred to evaporate the water for several hours until homogenous gel was formed. The gel was dried at 100 °C after it was aged overnight. The dried precursor was decomposed at 350 °C under nitrogen atmosphere for 4 h. The pre-heated precursor was grounded and reacted at 800 °C for 8 h under nitrogen atmosphere. The samples produced are simply named as LVMP-A, LVMP-B, LVMP-C and LVMP-D according to the doping reagents of MnO_2, MnOOH, Mn_3O_4 and $(CH_3COO)_2Mn\cdot 4H_2O$, respectively.

2.4. Characterization

All X-ray studies are done on a done on a Rigaku diffractometer (Dmax-2200) with Cu Kα radiation at 30 kV and 30 mA. The diffraction data are collected for 4 s at each 0.02° step from 10 to 80°. The morphology is investigated by field emission scanning electron microscope (FE-SEM, SIGMA, ZEISS).

2.5. Electrochemical measurement

The electrochemical characterizations were carried out using coin cell (CR2016). The composite cathode was formulated with active materials (80 wt%), Super P (10 wt%) and poly (vinylidene fluoride) (10 wt%) mixed in N-methyl-2-pyrrolidone. After stirred overnight, the slurry was cast onto Al foil by using a doctor blade, and dried at 120 °C for 12 h under vacuum. The weight loading of the cathode electrode is about 4 mg cm^{-2}. The coin cells were assembled in an argon-filled glove box using lithium metal as the negative electrode, Celgard 2500 as the separator, and 1 M $LiPF_6$ (dissolved in ethylene carbonate, dimethyl carbonate and ethyl-methyl carbonate with a 1:1:1 volume ratio) as the electrolyte. The galvanostatic charge and discharge experiments were made at room temperature (25 °C) by using LAND CT2001A (Wuhan, China) within the voltage range 3.0–4.3 V (1 C = 133 mAh g^{-1} *vs.* Li^+/Li), and 3.0–4.8 V (1 C = 197 mAh g^{-1} *vs.* Li^+/Li), respectively. Cyclic voltammetry (CV) was conducted on PARSTAT2273 electrochemical workstation at the scanning rate of 0.1 mV s^{-1} in the potential ranges of 3.0–4.5 V and 3.0–4.8 V (*vs.* Li^+/Li), respectively. A lithium foil acted as both the counter electrode and reference electrode. Electrochemical impedance spectroscopy (EIS) measures were carried out at the fresh state on PARSTAT2273 electrochemical workstation with sinusoidal signal of 5 mV over a frequency range from 100 kHz to 10 mHz.

3. Results and discussion

3.1. Structure and morphology characterization

In this work, MnO_2, MnOOH, Mn_3O_4 and $(CH_3COO)_2Mn\cdot 4H_2O$ are selected to be the manganese ion donor. The SEM images of MnO_2, MnOOH and Mn_3O_4 are shown in Fig. 1. As presented in Fig. 1A–C, the as-prepared MnOOH (Fig. 1B) mainly exist in the form of thin rod compared with the regular spheres of MnO_2 (Fig. 1A) and Mn_3O_4 nanoparticles (Fig. 1C). The XRD pattern of as-prepared MnOOH (shown in Fig. 1D) can be readily indexed to a monoclinic phase (space group: $P2_1/c$) with lattice constants $a = 0.530$ nm, $b = 0.527$ nm, $c = 0.530$ nm, compatible with literature values (PDF 41-1379). The characteristic peaks of Mn_3O_4, as labeled in Fig. 1D, are in good agreement with space group $I4_1/amd$ (JCPDS no. 80-0382), and no other impure crystalline phases is observed.

Fig. 2 shows the XRD patterns of manganese-doped LVP by different manganese sources. The XRD patterns of LVMP-A and LVMP-B are well indexed with the monoclinic $Li_3V_2(PO_4)_3$ (JCPDS PDF no. 80-1517, the space group of $P2_1/n$). There are no impurity peaks corresponding to the characteristic Mn-contained phase. Manganese ion with the valences of +3 and +4 have been successfully inserted into the lattice of $Li_3V_2(PO_4)_3$ to form a stable

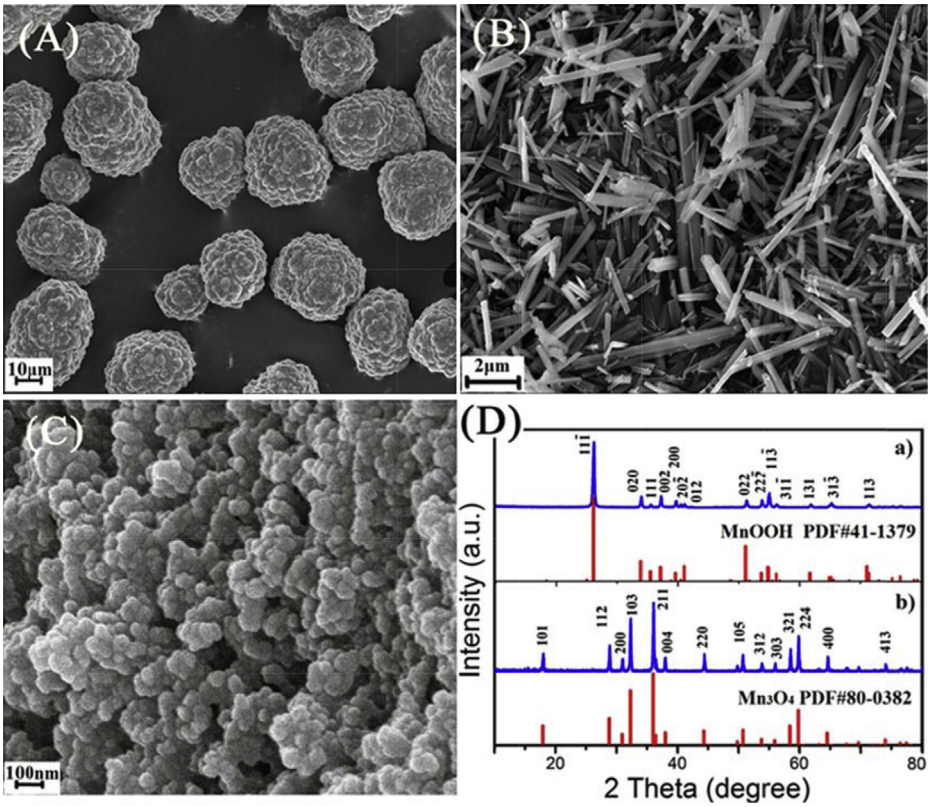

Fig. 1. SEM pictures of (A) commercial MnO_2, (B) as-prepared MnOOH and (C) as-prepared Mn_3O_4; (D) the XRD profiles of a) MnOOH and b) Mn_3O_4 and standard data from JCPDS no. 41-1379 and JCPDS no. 80-0382.

solid-solution even the substitution mole ratio reaches to 0.2. But the XRD patterns of LVMP-C and LVMP-D present the impurity phase of $LiMnPO_4$ when manganese ions with the valence of +2 involve in the substitution. The peaks noted in asterisk in LVMP-D show higher content of impurity $LiMnPO_4$ than those in LVMP-C.

Based on the XRD results and the crystal structure of monoclinic $Li_3V_2(PO_4)_3$, it is proper for Mn^{4+} provided by MnO_2 and Mn^{3+} provided by MnOOH to insert into the lattice of $Li_3V_2(PO_4)_3$ than Mn^{2+}/Mn^{3+} provided by Mn_3O_4. The monoclinic $Li_3V_2(PO_4)_3$ with PO_4 tetrahedral and VO_6 octahedral in NASICON structure, provides efficient three-dimensional pathways for Li^+ extraction and re-insertion [5,30]. When doped with Mn ion, the VO_6 octahedral are partly replaced by MnO_6 octahedral. Since the ionic radiuses of Mn^{4+}, Mn^{3+} and Mn^{2+} are 0.54, 0.62 and 0.76 Å, the Δr ($|r(Mn^{n+}) - r(V^{3+})|$) are 0.1, 0.02 and 0.12 Å, respectively, compared with V^{3+} (0.64 Å) in LVP. The small value of Δr is conducive to the Mn ion insert into the lattice of $Li_3V_2(PO_4)_3$ which occupies the V position to form a stable solid-solution, avoiding a large volume change of lattice. The refined unit cell lattice parameters for LVMP-A, LVMP-B, LVMP-C and LVMP-D are listed in Table 1. The lattice parameters vary dependently on the manganese sources, for example, the lattice parameter a is 8.5648, 8.6201, 8.6157 and 8.6147 Å of LVMP-A, LVMP-B, LVMP-C and LVMP-D, compared with 8.5539 Å of pure LVP. The biggest Δr causing the largest volume change of LVMP cells, for example, the volumes are 877.46, 880.12, 889.00 and 890.15 $Å^3$ of LVMP-A, LVMP-B, LVMP-C and LVMP-D, compared with 882.48 $Å^3$ of pure LVP, the ΔV ($|V$ (LVP) $- V$ (LVMP)|) is 5.02, 2.36, 6.52 and 7.67 $Å^3$, respectively. Because too

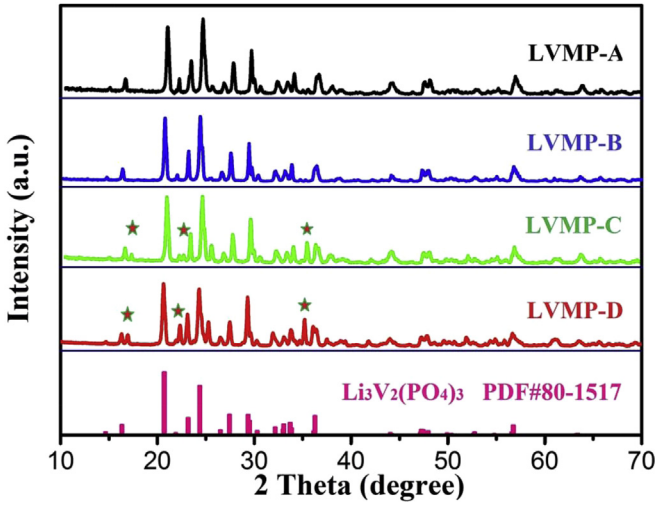

Fig. 2. XRD patterns of $Li_3V_{1.8}Mn_{0.2}(PO_4)_3$/C nanocomposites with different Mn-doping sources and the standard data of $Li_3V_2(PO_4)_3$ from JCPDS no. 80-1517, The peaks noted in asterisk show the phase of $LiMnPO_4$.

Table 1
Refined unit cell lattice parameters for LVMP samples.

Samples	a (Å)	b (Å)	c (Å)	β (deg)	V ($Å^3$)	$\lvert\Delta V\rvert$ ($Å^3$)
LVP[a]	8.5539	8.6099	11.9825	90.002	882.48	–
LVMP-A	8.5648	8.5643	11.9661	91.455	877.46	5.02
LVMP-B	8.6201	8.5938	11.8834	91.205	880.12	2.36
LVMP-C	8.6157	8.5905	12.0120	90.615	889.00	6.52
LVMP-D	8.6147	8.5945	12.0232	90.578	890.15	7.67

[a] Data came from Ref. [31].

much impurity phase, the studies of LVMP-D doped by Mn^{2+} are not shown in the following.

The XPS test conducts to analyze the valences of Mn ions in the structure of lithium vanadium phosphate. The XPS spectra of Mn 2p in LVMPs and the fitted data are illustrated in Fig. 3. The Mn 2p XPS spectrum of LVMPs exhibit two peaks at ~653 and ~641 eV, corresponding to Mn $2p_{1/2}$ and Mn $2p_{3/2}$ spin-orbit states of Mn, respectively (LVMP-C as example is shown in Fig. 3a). The fitted curves of Mn $2p_{3/2}$ of LVMP-A, LVMP-B and LVMP-C are plotted in Fig. 3b–d. It inevitably leads to the existence of minor Mn^{2+} since the reduction of carbon. The contents of Mn ions in different valences are calculated according to the area of the fitted peaks and the results are listed in the inset in Fig. 3, for example, the contents of Mn^{2+} and Mn^{4+} in LVMP-A are 18.13 and 81.87%. Mn^{2+} exists in all three samples as expected, but the main valence state of Mn ions in LVMP-A, LVMP-B and LVMP-C are Mn^{4+}, Mn^{3+} and Mn^{2+}, respectively.

Fig. 4 shows SEM images and elemental distribution mappings for the elements and the energy dispersive X-ray (EDX) spectrum of LVMP. The EDX of LVMP-A is shown in Fig. 4d, because others present the same results and don't show here. Fig. 4a–c shows the morphology of manganese-doped LVP with different Mn-sources. LVMP-A shows irregular particles with fluffy structure and large distribution of particles size, LVMP-B shows the homogenous nanoparticles, and blocky-shaped particles with large size presented in LVMP-C. The results of EDX measurement reveal that LVMP-A, LVMP-B and LVMP-C have the ratio of V/Mn is 13.8:1, 13.8:1 and 12:1 respectively, and those in precursor is 9:1. The deviation might be come from the different ratio of V/Mn on the inside and the outside of particles. Scanning SEM-EDX was utilized to verify the elemental composition of LVMP-A, LVMP-B and LVMP-C, as well as the nanoscale spatial uniformity of element distribution. All the elements (only Mn is shown in Fig. 4a'–c') are homogeneously distributed on manganese-doping LVP.

3.2. Electrochemical properties of LVMP in the voltage range 3.0–4.3 V

Cyclic voltammetry profiles (CVs) of Mn-doped LVP with different Mn sources are performed and plotted in Fig. 5. The three couples of redox peaks at about 4.15/3.96, 3.72/3.60 and 3.63/3.50 V are corresponding to three compositional regions of $Li_{3-x}V_2(PO_4)_3$ ($x = 0–0.5$, $x = 0.5–1.0$ and $x = 1.0–2.0$), respectively [30,31]. In the anodic process, the anodic peaks of LVMP-A and LVMP-C shift lower voltage compared with those of LVMP-B. The main difference of CVs among the three Mn-doped LVP samples is the potential interval (ΔE) between anodic and cathodic peaks. In general, the well-defined peaks and smaller value of ΔE always show the good reaction reversibility and lower ohmic resistance in the electrode reaction. As shown in Fig. 5, LVMP-B shows the lowest value of ΔE than the values in LVMP-A and LVMP-C. For example, ΔE of the couple near 4.15/3.96 V, corresponding to the second Li extraction/reinsertion, is 0.4 V in LVMP-A, 0.2 V in LVMP-B and 0.34 V in LVMP-C, respectively. LVMP-B by MnOOH as doping source exerts a more symmetrical and sharp shape of the anodic/cathodic peaks than the other two samples under the same synthetic conditions and doping ratio.

To find the effect of manganese sources in the electrochemical properties of Mn-doped LVP, the diffusion coefficients of Li^+ of LVMP are calculated based on electrochemical impedance spectroscopy (EIS). EIS has been widely used to identify the charge transfer resistance [32,33]. In this work, the batteries have been galvanostatically cycled for 2 cycles in the range of 3.0–4.3 V to ensure the percolation of the electrolyte through electrode particles. As shown in Fig. 6a–c, the impedance spectra obtained at different state of charge (SOC) 3.64, 3.85, 4.30, and 3.0 V are corresponding to the lithium extraction of $x = 0.5$, $x = 1.0$ and $x = 2.0$ in $Li_{3-x}V_2(PO_4)_3$, respectively. The Nyquist plots of the three samples exhibit a semicircle in the high frequency with a slope line in the low frequency region. The semicircle can be attributed to the

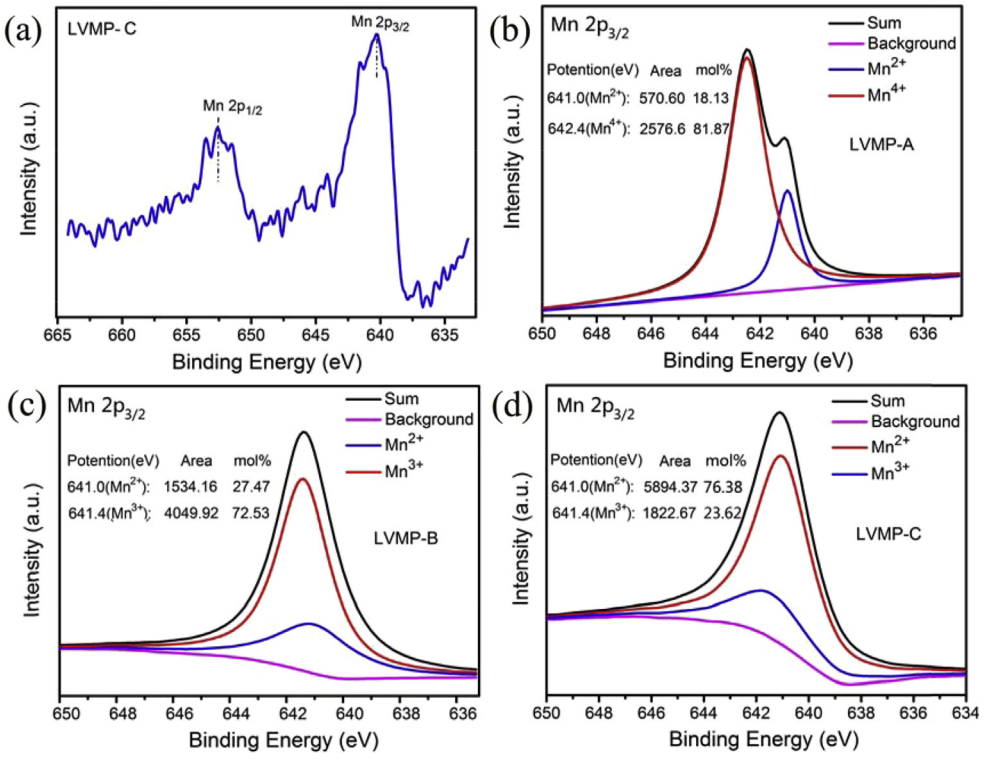

Fig. 3. XPS spectra of Mn 2p of LVMP-C (a), and the fitted XPS Mn $2p_{3/2}$ spectrum of LVMP-A (b), LVMP-B (c) and LVMP-C (d).

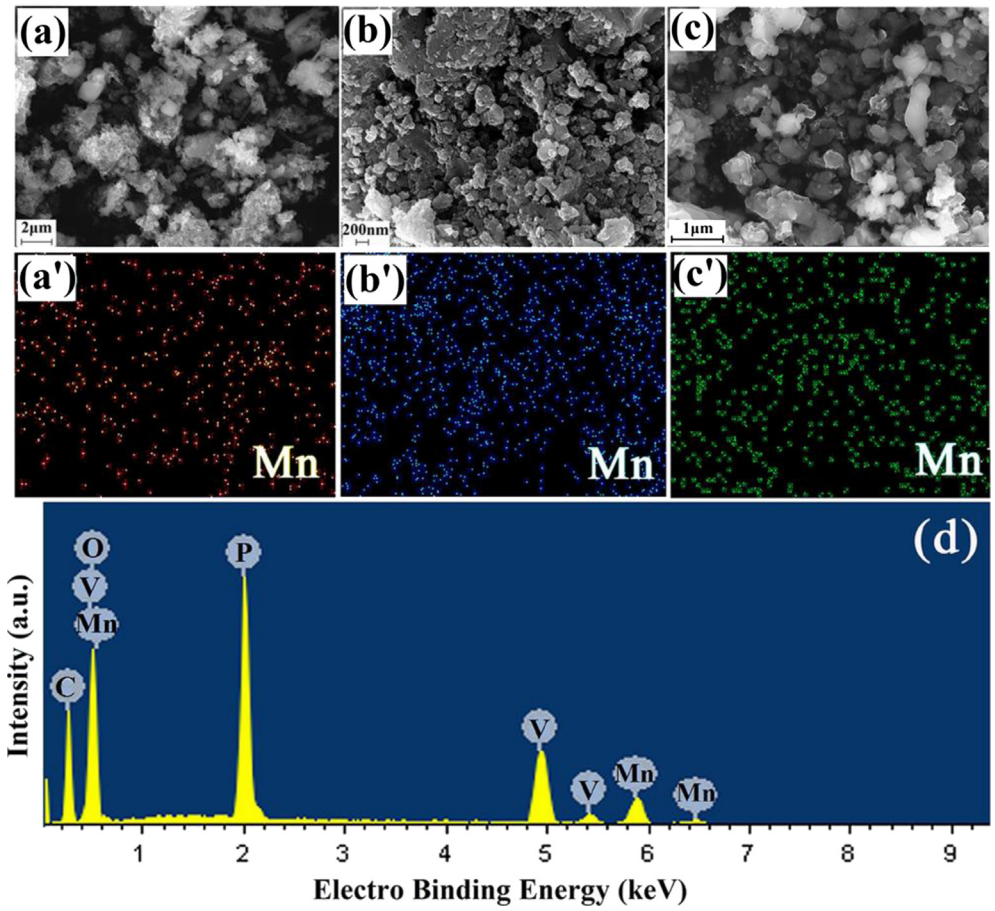

Fig. 4. SEM and scanning SEM elemental distribution mapping for Mn of (a), (a') LVMP-A; (b), (b') LVMP-B; and (c), (c') LVMP-C; (d) Energy dispersive X-ray spectrum of LVMP-A.

charge transfer reaction that represents the resistance of the lithium ion migration through the interface between the surface layer of the particles and the electrolyte. The low-frequency tail is attributed to the lithium diffusion in the solid phase and the Warburg resistance. The EIS of LVMP-A, LVMP-B and LVMP-C are dependent on the SOC of electrode as shown in Fig. 6a–c. LVMP-B presented the lowest high-frequency resistance at various SOC than

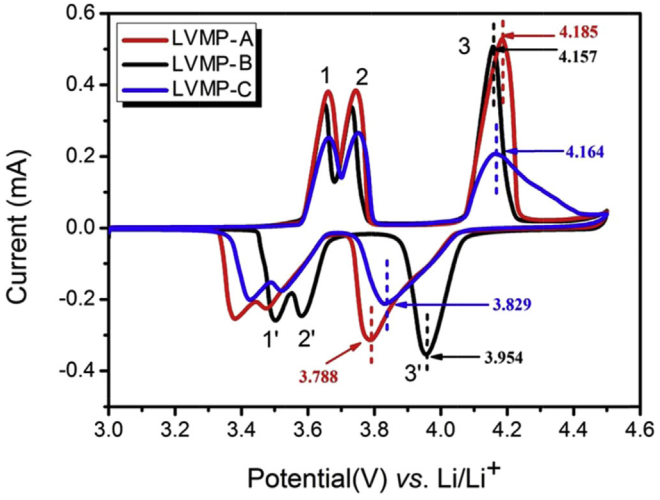

Fig. 5. Cyclic voltammetry profiles of LVMP electrodes at a scanning rate of 0.1 mV s^{-1} between 3.0 and 4.5 V.

LVMP-A and LVMP-C, for example, 85, 72 and 198 Ω in LVMP-A, LVMP-B and LVMP-C after the first 0.5Li extraction, 285, 151 and 600 Ω in LVMP-A, LVMP-B and LVMP-C after full discharge.

Based on the Nyquist plots, the Li^+ diffusion coefficients at different SOC are calculated according to the following equation [34,35]

$$D_{Li} = R^2T^2/2A^2F^2n^4C^2\sigma^2 \quad (1)$$

where D_{Li} is the diffusion coefficient of lithium ion, R is the gas constant, T is the absolute temperature, A is the surface area of the positive electrode, n is the number of transferred electron(s) per molecule during oxidization, F is the Faraday's constant, C is the lithium concentration in cathode material, and σ is the Warburg factor which is obtained from the slop of Z_{re} *vs.* reciprocal square root of frequency in the low frequency region ($\omega^{-1/2}$). Manganese sources as dopants play the important role in D_{Li^+} of LVP. It could be found that the D_{Li^+} of LVMP-B are much bigger than the values of LVMP-A and LVMP-C (as listed in Table 2). For example, at the SOC of 3.64 V the D_{Li^+} of LVMP-A, LVMP-B and LVMP-C are 7.8 × 10^{-11}, 20.1 × 10^{-11} and 2.6 × 10^{-11} cm^2 s^{-1}, respectively. LVP doped by proper Mn source presents improved lithium diffusion ability.

The electrochemical performance of LVMP is evaluated in half-cell at 3.0–4.3 V (*vs.* Li/Li^+), and Fig. 7a shows the initial charge/discharge profiles of LVMP-A, LVMP-B and LVMP-C at 0.1 C (1 C = 133 mAh g^{-1}). All the samples synthesized using the different manganese sources present three couples of voltage plateaus at ~3.60, ~3.68 and ~4.06 V, corresponding to extraction/reinsertion of 0.5Li, 0.5Li and the second Li of LVP. As shown in

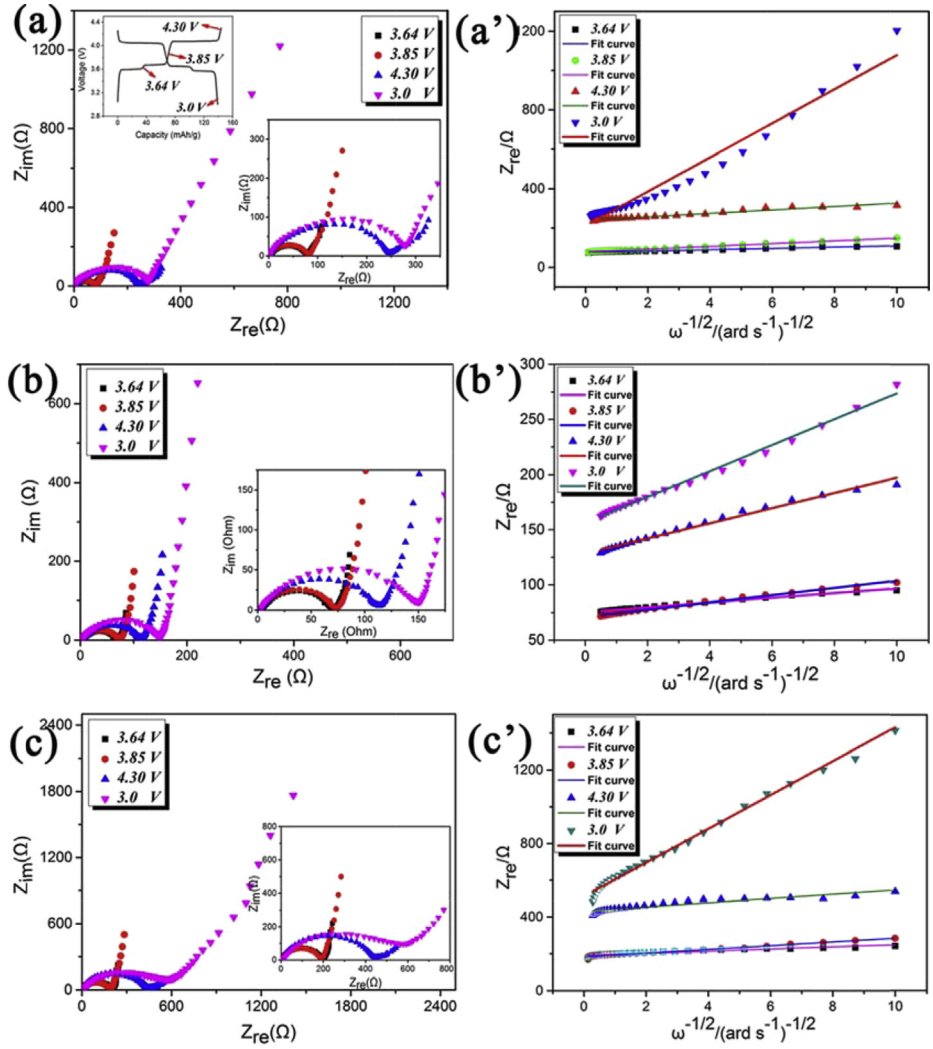

Fig. 6. Nyquist plots at different SOC and the plots of the real resistance as a function of the inverse square root of angular frequency: (a) LVMP-A, (b) LVMP-B and (c) LVMP-C in the range of 3.0–4.3 V.

Fig. 7a, LVMP-B delivered the highest capacity of 137 mAh g^{-1}, than LVMP-A 125 mAh g^{-1} of and LVMP-C 123 mAh g^{-1}. LVMP-B shows the best cycle performance, remaining 98% of the initial capacity after 50 cycles (as shown in Fig. 7b). MnOOH as doping reagent is much better than MnO_2 and Mn_3O_4. Mn source of MnOOH properly substituted the structure of LVP enhances the lithium diffusion ability and stability of LVP during charge/discharge.

Fig. 8 shows the rate performance of LVMP-A, LVMP-B and LVMP-C at the current densities of 0.1, 1, 2, 5 and 10 C, respectively. LVMP-A and LVMP-C exhibit poor rate performances along with the increase of current rates. For example, LVMP-A delivers capacities of 125, 107, 103, 74 and 37 mAh g^{-1} and LVMP-C delivers 124, 88, 40, 3, 3 mAh g^{-1} at the current rates of 0.1, 1, 2, 5 and 10 C, respectively. Only LVMP-B shows excellent rate performance of 138, 132, 131, 129 and 125 mAh g^{-1} at the current rates of 0.1, 1, 2, 5 and 10 C, respectively. After 35th charge/discharge cycles from 0.1 to 10 C-rate, the discharge capacities of LVMP-A, LVMP-B and LVMP-C at the 36th cycle are reproducible to 120, 135 and 120 mAh g^{-1} at the current rate of 0.1 C (as shown in Fig. 8a). The rate capacity retention at various current densities is presented in Fig. 8b. LVMP-B shows the best rate capacity retention, even carries out at high current density. For example, the capacity retention of LVMP-A, LVMP-B and LVMP-C are 65%, 93% and 2% at 5 C-rate, respectively.

Table 2
The calculated diffusion coefficients of Li^+ at various SOC.

SOC (V)	D_{Li^+} (10^{-11} cm^2 s^{-1})			
	3.64 V	3.85 V	4.30 V	3.0 V
LVMP-A	7.8380	1.7930	0.0733	0.0005
LVMP-B	20.077	8.4236	0.1167	0.0025
LVMP-C	2.5810	0.8495	0.0423	0.0004

3.3. Electrochemical properties of LVMP in the voltage range 3.0–4.8 V

One of the main problem of the cathode $Li_3V_2(PO_4)_3$ is the poor capacity and cycle performance in the voltage range 3.0–4.8 V, because the NASICON structure becomes unstable accompanying the extraction/reinsertion of the third lithium ion [30,31,36]. To investigate the full extraction/reinsertion of lithium ions, the electrochemical studies of LVMP are carried out in the voltage range 3.0–4.8 V.

Fig. 9 shows the CV profiles of LVP doped by three kinds of manganese sources in the voltage range 3.0–4.8 V. The three

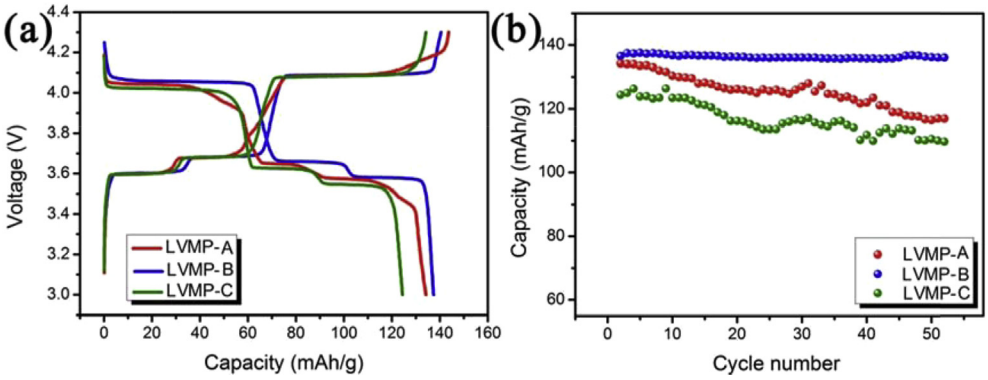

Fig. 7. Initial charge/discharge profiles and cycle performance of LVMP-A, LVMP-B and LVMP-C in the voltage range 3.0–4.3 V.

samples present four couples of redox peaks, corresponding to four compositional regions of $Li_{3-x}V_2(PO_4)_3$ (x = 0–0.5, x = 0.5–1.0, x = 1.0–2.0, and x = 2.0–3.0), respectively [30,31]. In the anodic process, the anodic peaks of LVMP-A and LVMP-C become overlap because the poor reversibility of reinsertion of lithium ions. The CVs of LVMP-B presents the strongest peak current and the distinguishable redox couples due to the improved lithium diffusion ability by the substitution of manganese from the dopant of MnOOH.

The diffusion coefficients of the third Li^+ during the charge/discharge process can also be calculated through electrochemical impedance spectroscopy (EIS) when the cells operated at 4.8 V. Fig. 10 presents the Nyquist plots of different SOC of the LVMP in the range of 3.0–4.8 V and the plots of the real resistance as a function of the inverse square root of angular frequency. The calculated D_{Li^+} based on Equation (1) lists in Table 3.

As listed in Table 3, the D_{Li^+} is decreased along with the extraction of lithium ions. For example, the values D_{Li^+} of 30.4×10^{-11}, 3.4×10^{-11}, 1.5×10^{-12} and 2.4×10^{-13} $cm^2\ s^{-1}$ in LVMP-B correspond to the extraction of 0.5Li, 0.5Li, 1Li and the last lithium ion, respectively. At the full charge (SOC = 100%), the extraction of the last lithium ion is hard out of the NASICON structure of LVP, and the extraction of the last lithium ion presents the smallest value of D_{Li^+} 2.4×10^{-13} $cm^2\ s^{-1}$. Likewise, at the full discharge state (SOC = 0), the electrode of LVMP-B presents the lowest value of D_{Li^+}, indicating the hard reinsertion of the third lithium ion, from $Li_2V_2(PO_4)_3$ phase to $Li_3V_2(PO_4)_3$ phase.

Compared with the values of D_{Li^+} in LVMP-B, those of LVMP-A and LVMP-C are much lower. It further indicates that MnOOH as dopant provides proper manganese substitution and enhance the lithium diffusion ability of LVP.

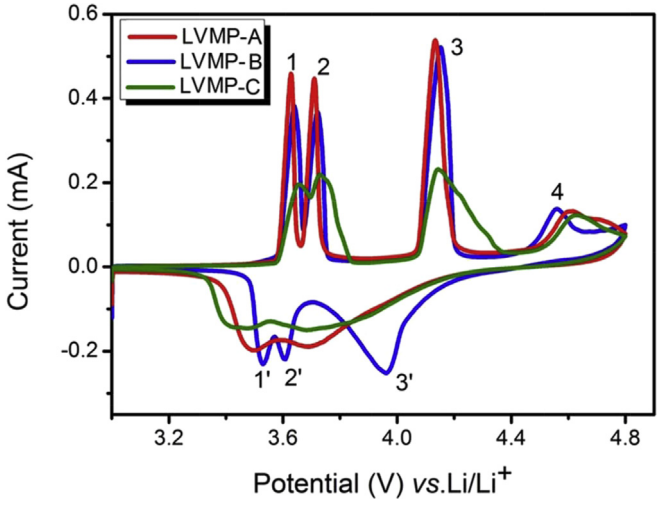

Fig. 9. Cyclic voltammetry profiles of LVMP electrodes at a scanning rate of 0.1 mV s^{-1} between 3.0 and 4.8 V.

The galvanostatic cycling profiles of LVMP samples are evaluated between 3.0 and 4.8 V at 0.1 C (1 C = 198 mAh g^{-1}) and are displayed in Fig. 11. As shown in Fig. 11a, four plateaus of the three samples clearly present during charge process, corresponding to the lithium extraction of 0.5Li, 0.5Li, 1Li, 1Li, respectively. In terms of the initial discharge capacity, the different manganese sources play distinguishing effect in the electrochemical properties in LVMP samples. The half-cells display discharge capacities of 167, 196 and 166 mAh g^{-1} in LVMP-A, LVMP-B and LVMP-C, respectively. Fig. 11b

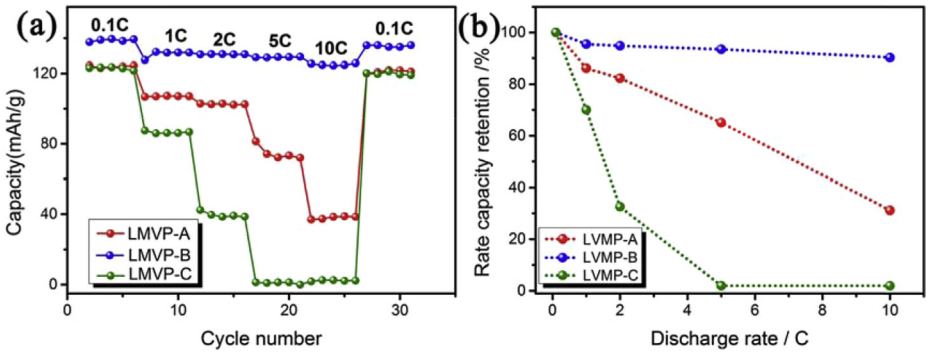

Fig. 8. Rate performance of LVMP-A, LVMP-B and LVMP-C in the voltage range 3.0–4.3 V.

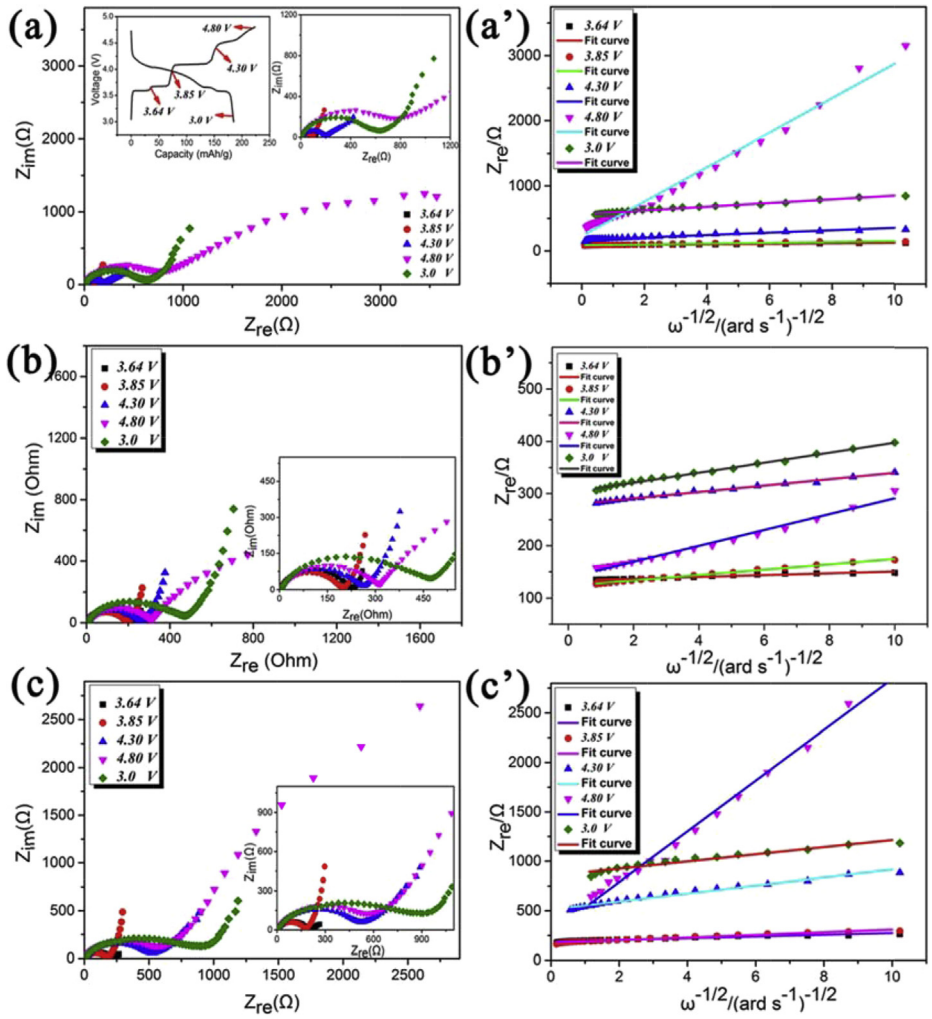

Fig. 10. Nyquist plots at different SOC and the plots of the real resistance as a function of the inverse square root of angular frequency: (a), (a') LVMP-A; (b), (b') LVMP-B and (c), (c') LVMP-C, in the voltage range 3.0–4.8 V.

shows the cycle performance of three LVMPs. After 50 cycles, LVMP-B still delivers 169 mAh g^{-1} (84% of the initial discharge capacity), much higher than LVMP-A of 137 mAh g^{-1} and LVMP-C of 127 mAh g^{-1}, respectively.

The rate performance of the three samples is shown in Fig. 12. There is significant capacity loss of LVMP-A and LVMP-C in the voltage range 3.0–4.8 V, but LVMP-B presents relative good rate performance. For example, LVMP-B delivers 190, 152, 143, 132 and 118 mAh g^{-1} at 0.1, 1, 2, 5 and 10 C-rate, respectively. LVMP-A and LVMP-C show the poor rate performance, such as 65 and 28 mAh g^{-1} at 5 C-rate, compared with 132 mAh g^{-1} of LVMP-B. After the electrodes cycled at high rate of 10 C-rate, it is interesting that LVMP-A, LVMP-B and LVMP-C almost return to the initial capacities at 0.1 C, except the poor high-rate performance of LVMP-A and LVMP-C. It further confirmed that Mn^{3+} of MnOOH as dopant improves the lithium diffusion ability and rate performance of LVP.

Table 3
The calculated diffusion coefficients of Li^+ at various SOC.

Samples	D_{Li^+} (10^{-11} cm^2 s^{-1})				
	3.64 V	3.85 V	4.30 V	4.80 V	3.0 V
LVMP-A	6.4350	2.2959	0.0164	0.00079	0.00007
LVMP-B	30.398	3.3910	0.1477	0.0239	0.0008
LVMP-C	1.1532	0.4889	0.0034	0.00084	0.00005

Fig. 12b shows the rate capacity retentions of LVMP samples. LVMP-B shows the best capacity retention than LVMP-A and LVMP-C. Except the poor high-rate performance, LVMP-B also presents normal high-rate performance in the voltage range 3.0–4.3 V compared with the value obtained in the range of 3.0–4.8 V. For example, the capacity of LVMP-B at 5 C-rate shows 71% of the 0.1 C-rate capacities in range 3.0–4.8 V, lower than value 93% of the 0.1 C-rate capacities in range 3.0–4.3 V (as shown in Fig. 8b). It might due to the following reasons: the electrolyte oxidation occurred in the large electrochemical window (3.0–4.8 V); the as-synthesized samples LVMP might be a little dissolved under relative higher voltage; and the crystal structure of $V_2(PO_4)_3$ and $LiV_2(PO_4)_3$ is distorted during the phase transition process at the high voltage (>4.6 V) [4]. The dopant of MnOOH provided Mn^{3+} substitution in LVP plays positive effect to stables the structure change between $V_2(PO_4)_3$ and $LiV_2(PO_4)_3$ than others dopants of MnO_2 and Mn_3O_4.

Based on the above discussions, the selection of manganese sources plays an important role in improving the electrochemical performances of LVP. The value of Δr ($|r(Mn^{n+}) - r(V^{3+})|$) is a key consideration when choosing the manganese ion donor. The Mn^{3+} of MnOOH is a prefer dopant of LVP and improve the electrochemical properties of LVP.

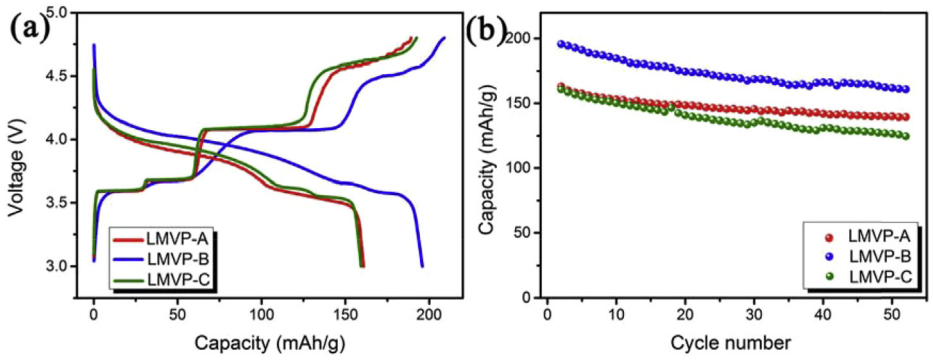

Fig. 11. Initial charge/discharge profiles and cycle performance of LVMP-A, LVMP-B and LVMP-C in the voltage range 3.0–4.8 V.

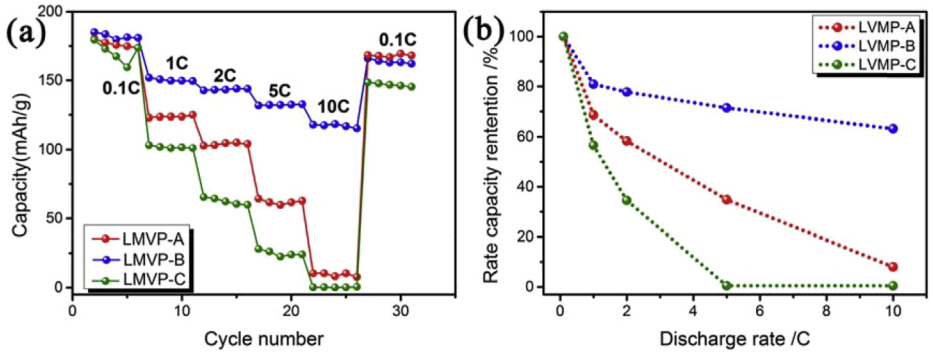

Fig. 12. Rate performance of LVMP-A, LVMP-B and LVMP-C in the voltage range 3.0–4.8 V.

4. Conclusion

The NASICON structured LVP doped by manganese ions are synthesized via sol–gel route by using four types of manganese dopants: MnO_2, MnOOH, Mn_3O_4 and $(CH_3COO)_2Mn{\cdot}4H_2O$. It is easier for Mn^{4+} provided by MnO_2 and Mn^{3+} provided by MnOOH to insert into the lattice of $Li_3V_2(PO_4)_3$ to form a stable solid-solution than Mn^{2+}/Mn^{3+} provided by Mn_3O_4, because the later presents a lot of impurity phase of $LiMnPO_4$. Mn^{2+} exists in all three samples as expected since reduction of carbon, but the main valence state of Mn ions in LVMP-A, LVMP-B and LVMP-C are Mn^{4+}, Mn^{3+} and Mn^{2+}, respectively. Compared with V^{3+} (0.64 Å) in LVP, the Δr ($|r(Mn^{n+})$ (n = 4, 3, 2) − $r(V^{3+})|$) are 0.1, 0.02 and 0.12 Å, respectively. The manganese source owning the smallest value of Δr causes the smallest volume changes of VO_6 octahedra. LVMP-B (MnOOH as dopant) delivers the highest capacity of 137 mAh g^{-1}, than LVMP-A (MnO_2 as dopant) 125 mAh g^{-1} of and LVMP-C (Mn_3O_4 as dopant) 123 mAh g^{-1}. LVMP-B shows the best cycle performance, remaining 98% of the initial capacity after 50 cycles (in range 3.0–4.3 V). Mn source of MnOOH properly substituted the structure of LVP enhances the lithium diffusion ability, high-rate performance and stability of LVP during charge/discharge.

Acknowledgments

The work was sponsored by Qing Lan Project, and NSF of China (Grant no. 51172032, 11174043).

References

[1] H.D. Liu, G. Yang, X.F. Zhang, P. Gao, L. Wang, J.H. Fang, J. Pinto, X.F. Jiang, J. Mater. Chem. 22 (2012) 11039–11047.
[2] J. Shirakawa, M. Nakayama, M. Wakihara, Y. Uchimoto, J. Phys. Chem. B 110 (2006) 17743–17750.
[3] Q. Kuang, Y.M. Zhao, Z.Y. Liang, J. Power Sources 196 (2011) 10169–10175.
[4] S. Patoux, C. Wurm, M. Morcrette, G. Rousse, C. Masquelier, J. Power Sources 119 (2003) 278–284.
[5] S.C. Yin, H. Grondey, P. Strobel, M. Anne, L.F. Nazar, J. Am. Chem. Soc. 125 (2003) 10402–10411.
[6] H.D. Liu, P. Gao, J.H. Fang, G. Yang, Chem. Commun. 47 (2011) 9110–9112.
[7] L.L. Zhang, X. Zhang, Y.M. Sun, W. Luo, X.L. Hu, X.J. Wu, Y.H. Huang, J. Electrochem. Soc. 158 (2011) A924–A929.
[8] S.Q. Liu, S.C. Li, K.L. Huang, Z.H. Chen, Acta Phys. Chim. Sin. 23 (2007) 537–542.
[9] M. Sato, H. Ohkawa, K. Yoshida, M. Saito, K. Uematsu, K. Toda, Solid State Ionics 135 (2000) 137–142.
[10] M.M. Ren, Z. Zhou, Y.Z. Li, X.P. Gao, J. Yan, J. Power Sources 162 (2006) 1357–1362.
[11] A.R. Cho, J.N. Son, V. Aravindan, H. Kim, K.S. Kang, W.S. Yoon, W.S. Kim, Y.S. Lee, J. Mater. Chem. 22 (2012) 6556–6560.
[12] J.N. Son, G.J. Kim, M.C. Kim, S.H. Kim, V. Aravindan, Y.G. Lee, Y.S. Lee, J. Electrochem. Soc. 160 (2013) A87–A92.
[13] J.H. Yao, S.S. Wei, P.J. Zhang, C.Q. Shen, K.F.A. Zinsou, L.B. Wang, J. Alloys Compd. 532 (2012) 49–54.
[14] Y.H. Chen, Y.M. Zhao, X.N. An, J.M. Liu, Y.Z. Dong, L. Chen, Electrochim. Acta 54 (2009) 5844–5850.
[15] C.W. Sun, S. Rajasekhara, Y.Z. Dong, J.B. Goodenough, ACS Appl. Mater. Interfaces 3 (2011) 3772–3776.
[16] S.K. Zhong, L.T. Liu, J.Q. Jiang, Y.W. Li, J. Wang, J.Q. Liu, Y.H. Li, J. Rare Earths 27 (2009) 134–137.
[17] J.S. Huang, L. Yang, K.Y. Liu, Y.F. Tang, J. Power Sources 195 (2010) 5013–5018.
[18] C. Dai, Z. Chen, H. Jin, X.G. Hu, J. Power Sources 195 (2010) 5775–5779.
[19] T. Zhai, M.S. Zhao, D.D. Wang, Trans. Nonferrous Met. Soc. China 21 (2011) 523–528.
[20] M. Bini, S. Ferrari, D. Capsoni, V. Massarotti, Electrochim. Acta 56 (2011) 2648–2655.
[21] Q. Kuang, Y. Zhao, X. An, J.M. Liu, Y.Z. Dong, L. Chen, Electrochim. Acta 55 (2010) 1575–1581.
[22] M. Yoshioa, Y. Todorova, K. Yamatoa, H. Noguchia, J. Itoha, M. Okadab, T. Mourib, J. Power Sources 74 (1998) 46–53.
[23] L.L. Zhang, X.B. Zhang, Z.L. Wang, J.J. Xu, D. Xua, L.M. Wang, Chem. Commun. 48 (2012) 7598–7600.
[24] C.J. Pan, Y.J. Lee, B. Ammundsen, C.P. Grey, Chem. Mater. 14 (2002) 2289–2299.
[25] Z.C. Bai, N. Fan, Z.C. Ju, C.H. Sun, Y.T. Qian, Mater. Lett. 76 (2012) 124–126.

[26] L. He, S.C. Zhang, X. Wei, Z.J. Du, G.R. Liu, Y.L. Xing, J. Power Sources 220 (2012) 228–235.
[27] C. Deng, S.Y. Yang, Y. Gao, B. Wu, L. Ma, B.L. Fu, Q. Wu, F.L. Liu, J. Phys. Chem. C 115 (2011) 15048–15056.
[28] S. Feth, G.V. Gibbs, M.B. Boisen Jr., R.H. Myers, J. Phys. Chem. 97 (1993) 11445–11450.
[29] L. Wang, Y.H. Li, Z.D. Han, L. Chen, B. Qian, X.F. Jiang, J. Pinto, G. Yang, J. Mater. Chem. A 1 (2013) 8385–8397.
[30] H. Huang, S.C. Yin, T. Kerr, N. Taylor, L.F. Nazar, Adv. Mater. 14 (2002) 1525–1528.
[31] S.C. Yin, H. Grondey, P. Strobel, H. Huang, L.F. Nazar, J. Am. Chem. Soc. 125 (2003) 326–327.
[32] X.H. Rui, N. Ding, J. Liu, C. Li, C.H. Chen, Electrochim. Acta 55 (2010) 2384–2390.
[33] P. Gao, Y.H. Li, H.D. Liu, J. Pinto, X.F. Jiang, G. Yang, J. Electrochem. Soc. 159 (2012) A1–A8.
[34] H. Liu, C. Li, H.P. Zhang, L.J. Fu, Y.P. Wu, H.Q. Wu, J. Power Sources 159 (2006) 717–720.
[35] H. Liu, Q. Cao, L.J. Fu, C. Li, Y.P. Wu, H.Q. Wu, Electrochem. Commun. 8 (2006) 1553–1557.
[36] G. Yang, H.M. Ji, H.D. Liu, B. Qian, X.F. Jiang, Electrochim. Acta 55 (2010) 3669–3680.